Research Article

Journal of Environmental Nanotechnology

Comparative Analysis of Nano-CPH Reinforced Brake Pad Composites: Mechanical, Tribological, and Morphological Investigations

M. Sathesh Babu[1*], K. Saravanan[2], U. Vivek[3] and S. N. Dinesh[4]

[1]Department of Mechanical Engineering, CMS College of Engineering and Technology, Coimbatore, TN, India
[2]Department of Mechanical Engineering, Akshaya College of Engineering and Technology, Coimbatore, TN, India
[3]Department of Mechanical Engineering, K. S. Rangasamy College of Technology, KSR Kalvi Nagar, Tiruchengode, TN, India
[4]Department of Mechanical Engineering, KPR Institute of Engineering and Technology, Coimbatore, TN, India
Received: 12.08.2025 Accepted: 23.09.2025 Published: 30.09.2025
*satheshbabum@gmail.com

ABSTRACT

This study investigates the potential of nanostructured cocoa pod husks (nano-CPH) as an eco-friendly filler in automotive brake pad composites. Nano-CPH was incorporated into epoxy-based composites at varying concentrations (16–31 wt. %) along with other constituents such as silica, iron oxide, calcium carbonate, and graphite. The mechanical, tribological, and morphological properties of the composites were evaluated using standardized tests and scanning electron microscopy (SEM). The results showed that the optimal composition, which contained 21 wt. % nano-CPH exhibited significantly enhanced tensile strength (31.2 MPa), compressive strength (70.6 MPa), and Shore A hardness (88.83) compared with other filler loadings. Tribological testing revealed that the 21 wt. % nano-CPH composites exhibited the most stable and highest friction force (10.2–17.5 N) and low wear depth (15 µm), which can be attributed to the formation of a uniform, lubricating transfer film. SEM analysis confirmed the homogeneous dispersion of nano-CPH and strong matrix–filler interfacial bonding at this optimal loading. Comparative analysis highlighted the superior mechanical and tribological performance of the nano-CPH composite over other bio-based brake pad materials. These findings demonstrate the viability of nano-CPH as a sustainable, high-performance filler for eco-friendly brake pad applications, thereby promoting the valorization of agricultural waste in the automotive industry.

Keywords: Nanostructured cocoa pod husk; Epoxy-based composites; Tensile strength; Compressive strength; Shore A hardness; Tribological performance; Automotive brake pad.

1. INTRODUCTION

Automotive brake pad composites play a vital role in vehicle safety by enabling controlled deceleration through the conversion of kinetic energy into heat through frictional forces (Kumar *et al.* 2021). Historically, these composites have relied heavily on a mix of metallic, ceramic, and synthetic fillers, with asbestos being the predominant filler material owing to its excellent thermal resistance, mechanical strength, and frictional stability (Nandiyanto *et al.* 2021; Onyenanu *et al.* 2024). However, the carcinogenic nature of asbestos has led to stringent regulations and bans worldwide, compelling researchers and manufacturers to seek safer and more sustainable alternatives (Imran *et al.* 2024). In addition to asbestos-related health concerns, conventional fillers such as metallic and synthetic fibers pose challenges related to high costs, environmental impact, and poor biodegradability (Chandradass *et al.* 2021; Bhakuni *et al.* 2023). These limitations underscore the urgent need for eco-friendly brake pad materials that maintain or exceed the performance characteristics of traditional composites while minimizing the environmental and health risks of the latter (Nandiyanto *et al.* 2022a; Dirisu *et al.* 2024).

In recent years, agro-waste-based fillers have emerged as promising alternatives in brake pad composites, attracting considerable attention owing to their sustainability, wide availability, renewability, and low cost (Pradhan *et al.* 2022; Chaturvedi *et al.* 2023; Divakaran *et al.* 2023; García-Mahecha *et al.* 2023; Kannan *et al.* 2024). Such materials effectively valorize agricultural by-products, reduce waste accumulation, and foster circular economy principles (Yashwhanth *et al.* 2021). Numerous studies have explored a variety of natural fibers and agro-waste fillers such as coconut shell (Navaneethakrishnan *et al.* 2021), palm kernel shell (Lokeshwari *et al.* 2022), bamboo (Kumar *et al.* 2025), rice husk (Prado and Spinacé, 2015; Nandiyanto *et al.* 2022b), banana peel (Pelissari *et al.* 2017), bush mango shell (Onyenanu *et al.* 2024), jute (Ahmad *et al.* 2022), sisal (Manjulaiah *et al.* 2024), and molluscan shells (Jiyas *et al.* 2025), which have demonstrated comparable or even superior mechanical, tribological, and thermal properties relative to conventional fillers. For instance, a

study by Adetunji *et al.* (2022) reported that coconut shell and palm kernel shell fillers significantly enhanced hardness, compressive strength, and wear resistance, while maintaining suitable friction coefficients. Similarly, Dagwa *et al.* (2025) showed that carbonized bamboo particles integrated into epoxy matrices exhibited excellent tensile strength, friction stability, and thermal resistance up to 950 °C. These findings highlight the capability of properly processed natural fillers to meet the rigorous demands of brake-pad applications.

Investigations into rice husks (Khafidh *et al.* 2023) and cocoa bean shells (Olabisi, 2016), and banana peel (Yigrem *et al.* 2022a) composites have shown notable tribological benefits. Nandiyanto *et al.* (2021) demonstrated that fine rice husk particles improved compressive strength and wear resistance, while Yigrem *et al.* (2022a) reported excellent mechanical and wear performance in banana peel/carbon composites, particularly as the carbon content increased. The incorporation of biochar derived from pyrolyzed agro-waste and biogenic ceramics, such as silicon nitride synthesized from sorghum husk, has also been shown to provide thermal and frictional advantages, serving as advanced eco-friendly friction modifiers (Manoj *et al.* 2024). Moreover, natural fiber reinforcements, such as sisal, jute, and kenaf, have been effectively hybridized to yield composites with enhanced compressive, flexural, and impact strengths, outperforming nonreinforced pads and approaching or exceeding the performance of commercial metallic pads (Manjulaiah *et al.* 2024).

Marine bio-waste fillers, including molluscan shells, are an innovative class of bio-fillers that contribute to stable friction and high wear resistance. Jiyas *et al.* (2025) showed that molluscan shell-based composites delivered friction coefficients comparable to commercial materials alongside thermal stability up to 800 °C, while reducing environmental impact during production and disposal. These diverse materials collectively illustrate the feasibility of using agro-waste and natural fibers as efficient and sustainable constituents in brake pad composites. The critical factors influencing their performance include particle size, filler content, and processing methods. Studies have consistently indicated that fine particles (<300 μm) enhance matrix-filler bonding, mechanical strength, hardness, and wear resistance, whereas coarse particles tend to introduce porosity, reduce mechanical integrity, and increase wear (Yigrem *et al.* 2022b; Ali *et al.* 2022; Yilma *et al.* 2023). Statistical optimization techniques, such as Response Surface Methodology (RSM) (Sivakumar and Saju, 2024) and Taguchi designs (Yilma *et al.* 2023), have been widely employed to determine optimal content ranges, with 30–45 wt. % natural filler loadings typically yielding the best composite properties.

Despite these promising findings, a distinct research gap remains concerning the application of cocoa pod husks (CPH), a widely available agro-waste by-product from cocoa cultivation and chocolate production, particularly at the nanoscale. Cocoa pod husk is primarily composed of lignin and cellulose, biopolymers known for their mechanical strength and thermal stability, making CPH a compelling candidate for inclusion in brake pad composites. Previous studies have investigated micro- and macro-scale CPH incorporation into polymer composites, reporting improved mechanical strength, thermal resistance, and wear properties owing to their fibrous structure and lignin content. For example, some researchers have successfully reinforced polymer matrices with raw or processed CPH and observed enhancements in the tribological and mechanical behaviors of the composites. However, these studies have largely overlooked the potential advantages of nanostructuring CPH to enhance further filler dispersion, interfacial adhesion, and stress transfer, which are critical for maximizing composite performance in demanding brake applications.

The importance of nanostructured fillers in polymer composites is well documented in the materials science literature, where reductions to the nanoscale often translate into superior mechanical and tribological properties owing to the increased surface area and improved interaction with the polymer matrix. However, systematic research exploring nano-CPH as an eco-friendly, high-performance reinforcement in brake pad systems remains scarce. Specifically, there is limited understanding of how nano-CPH affects the friction coefficient stability, wear rate reduction, mechanical strength improvement, and thermal degradation resistance under braking conditions. This lack of comprehensive data restricts the design and optimization of nano-CPH-based brake pad composites, impeding their development for industrial applications.

Motivated by this significant gap, the present study aims to investigate the effects of incorporating nano-CPH into automotive brake pad composites. This research focuses on developing and characterizing nano-CPH particles, analyzing their dispersion and interaction within polymer matrices, and evaluating the tribological, mechanical, and thermal properties of the resulting composites under simulated braking scenarios. The goal of this study is to demonstrate that nano-CPH can provide enhanced filler-matrix bonding, improve mechanical strength, reduce wear, and achieve stable friction performance while maintaining or improving thermal stability compared to conventional and micro-scale CPH composites.

This study is situated within the broader context of the automotive industry's increasing commitment to sustainability and environmental responsibility. Leveraging locally abundant agro-waste, such as cocoa pod husks, complements global efforts to reduce reliance on non-renewable, toxic materials and promote circular

economy principles. Furthermore, the integration of nanotechnology into natural filler processing represents a cutting-edge approach to reconcile the competing demands of ecological safety and high performance. By systematically addressing the processing, formulation, and performance evaluation challenges associated with nano-CPH in brake pads, this study offers valuable insights and practical solutions that can accelerate the transition to sustainable and high-performance automotive friction materials.

In conclusion, although conventional brake pad composites have historically delivered reliable performance, their environmental and health drawbacks necessitate urgent alternatives. Agro-waste fillers, such as cocoa pod husks, are promising substitutes owing to their renewability, eco-friendliness, and cost-effectiveness. The demonstrated benefits of CPH's lignocellulosic composition in prior studies confirm its potential; however, the untapped advantages of nanoscale structuring remain largely unexplored. This study aims to fill this critical knowledge gap by investigating the integration of nanostructured CPH into brake pad composites to produce safe, sustainable, and high-performing brake materials that meet industry standards and contribute positively to environmental goals.

2. MATERIALS AND METHODS

2.1 Materials

Epoxy resin (LY556) and hardener (HY951) served as the matrix system, providing strong bonding and thermal stability. Cocoa pod husks, an abundant agro-waste filler, offer sustainability benefits and mechanical reinforcement owing to their lignocellulosic nature. Silica and iron oxide function as abrasives to maintain friction and wear performance, whereas calcium carbonate acts as a cost-effective reinforcement to improve stiffness and dimensional stability. Powdered graphite was included as a friction modifier to enhance lubrication, reduce noise, and improve braking smoothness under varying conditions. A detailed justification of the selection of each material is provided in Table 1.

Table 1. Justification for material selection

S. No.	Materials	Reason for Selection
1	Matrix: Epoxy resin (LY556) + Hardener (HY951)	Though not conventionally employed in brake pad applications, this epoxy system was selected to investigate its potential as a binder due to its availability, relatively low cost, and ability to form strong cross-linked networks upon curing. It also provides thermal stability and good mechanical strength.
2	Filler: Cocoa pod husk (CPH)	It was chosen as a sustainable, agro-waste-derived filler readily found in Nigerian agricultural waste sites. Prior studies suggest its lignocellulosic structure contributes to thermal resistance and mechanical interlocking, making it a promising material in friction composites. Its eco-friendliness and low cost also make it attractive for industrial use.
3	Abrasives: Silica, iron oxide	These materials were selected for their proven abrasive qualities, which aid in maintaining surface roughness and friction coefficient consistency. They help form and stabilize the friction layer during braking, thereby enhancing wear performance.
4	Reinforcement: Calcium carbonate ($CaCO_3$)	Acts as a cost-effective substitute for barytes, offering good dispersion properties and promoting matrix-filler adhesion. Its role in improving the stiffness and dimensional stability of the composite under mechanical stress was also considered.
5	Friction modifier: Powdered graphite (75 µm)	Graphite was included due to its lubricating properties, particularly beneficial under wet or high-temperature conditions. It contributes to noise reduction, smoother braking action, and reduced wear, without posing health or environmental risks.

2.2 Sample Preparation

The cocoa pod husks were initially obtained from local agricultural waste sites in Pollachi, Tamil Nadu, India. They were meticulously cleaned using distilled water to eliminate surface impurities and subsequently dried in a hot air oven at 60 °C for a duration of 24 h. The dried cocoa pod husks were then ground into coarse particles using an electric blender and subsequently processed using high-energy ball milling at 450 rpm for 30 min to achieve nanoscale particle size reduction. The resulting nano-CPH powder was sieved through a 100-mesh sieve (<150 µm) to ensure uniform particle size. The epoxy resin (LY556) and hardener (HY951) were mixed at the manufacturer's recommended weight ratio of 100:84 (resin: hardener) to form the binding matrix. In a separate mixing vessel, measured quantities of nano-CPH powder (varying 10–30 wt. %), silica (15 wt. %), iron oxide (10 wt. %), calcium carbonate (20 wt. %), and graphite (5 wt. %) were dry-blended using a mechanical mixer at 150 rpm for 10 minutes to achieve a homogeneous distribution, as per the concoction listed in Table 2. The dry filler mixture was then gradually incorporated into the epoxy-hardener

solution under continuous mechanical stirring at 300 rpm for 15 min to ensure complete wetting and uniform dispersion of all components. The resulting composite mixture was degassed under vacuum at 0.1 MPa for 5 min to eliminate trapped air bubbles, and then poured into pre-cleaned and lubricated steel molds with dimensions of 30 mm × 30 mm × 5 mm, conforming to the standard brake pad test specimen requirements. The filled molds were subjected to compression molding at 15 MPa and 180 °C for 10 min, followed by gradual cooling to room temperature while maintaining the pressure. The molded specimens were then subjected to post-curing treatment at 120 °C for 2 h in a conventional oven to ensure complete cross-linking and optimal mechanical properties. After post-curing, the samples were cooled to ambient temperature and demolded at room temperature. Final specimen preparation involved light surface grinding with 120-grit emery paper to achieve a uniform surface finish and a precise dimensional tolerance of ±0.1 mm for subsequent characterization and performance testing. Fig. 1 shows the sequential steps involved in the preparation of the samples.

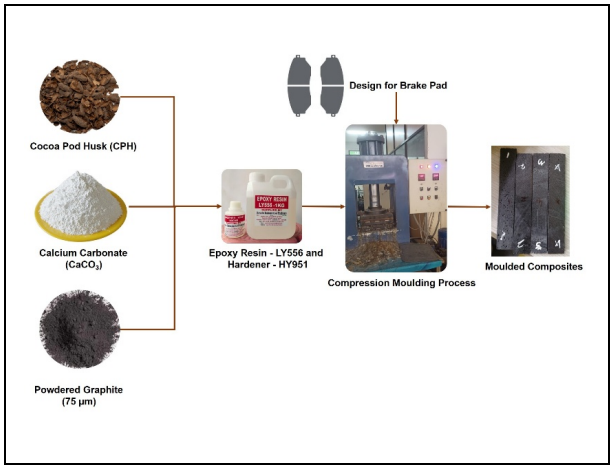


Fig. 1: Sequential steps for sample preparation

Table 2. Concoction for sample preparation

S. No.	Material	Composition 1 (wt. %)	Composition 2 (wt. %)	Composition 3 (wt. %)	Composition 4 (wt. %)
1	Epoxy resin + Hardener	50	55	60	65
2	Calcium carbonate ($CaCO_3$)	4	4	4	4
3	Cocoa pod husk (CPH)	31	26	21	16
4	Silica	7	7	7	7
	Iron oxide	3	3	3	3
5	Powdered graphite	5	5	5	5
	Total	100	100	100	100

2.3 Characterization Techniques

2.3.1 Characterization of CPH Nanofillers

2.3.1.1 FTIR Analysis

The chemical composition and functional groups of the extracted cocoa pod husk nanofillers were examined using FTIR spectroscopy (Jasco FT/IR-4000 Series). For sample preparation, 2 mg of powdered fiber was mixed with potassium bromide (KBr) and compressed into pellets. The spectra were obtained in reflectance mode at 30°C, covering the wavenumber range of 4000–400 cm-¹, with a spectral resolution of 4 cm^{-1} and a scanning rate of 32 scans/min.

2.3.1.2 XRD Analysis

The crystallization characteristics were examined by X-ray diffraction (XRD) technique using a D8 ADVANCE diffractometer equipped with monochromatic Cu-Kα radiation (operating voltage: 45 kV). Diffraction patterns were recorded at a scanning rate of 3°/min, with a step size of 0.02°. The collected data were processed and visualized in two-dimensional form using the Origin Pro software (version 2025b). The crystallinity index (CI) was determined using the peak deconvolution method described in Eq. (1).

$$CI\% = \frac{I_{crys} + I_{amp}}{I_{crys}} \text{ x } 100 \quad \ldots (1)$$

where, I_{crys} represents the intensity of the crystalline region, and I_{amp} corresponds to the intensity of the amorphous region. In addition, the diffraction angle was used to determine the crystallinity index using the Scherrer equation (Eq. 2),

$$D = \frac{k\lambda}{\beta \cos\theta} \quad \ldots (2)$$

where,

D - Crystallite size,
k - Scherrer constant
β - Full-width at half-maximum (FWHM)

λ - Wavelength of inclination
θ - Bragg angle of inclination.

2.3.1.3 Particle Size Analysis

The particle size distribution of the CPH was determined using the ImageJ image analysis software. Microscopic images of the CPH samples were acquired under consistent magnification and lighting conditions. The images were calibrated using a known scale bar to ensure accurate measurement. The particle boundaries were identified through threshold adjustment, and Feret's diameter (maximum caliper length) was measured for each particle. The recorded data were used to calculate the size distribution and average particle diameters.

2.3.2 Mechanical Characterization

The mechanical properties were evaluated using standardized tests. Shore A hardness measurements were conducted at five random points per specimen using a digital durometer (Yuzuki Shore A hardness tester, Model No.: DRHTA) under a 1-second dwell time, and the average value was reported. Tensile testing was performed following ASTM D638 (2014) using an Aimil Universal Testing Machine (UTM) at a crosshead speed of 2 mm/min; the specimens (Type I dog bone - 165 mm x 13 mm x 3.2 mm with a gauge length of 50 mm) yielded tensile strength, modulus, and elongation at break. The compressive strength was determined according to ASTM D695 (2023) on cylindrical specimens (12 mm × 6 mm) at 1.3 mm/min, measuring the peak load and the compressive modulus.

2.3.3 Tribological Characterization

The tribological performance was assessed using a Pin-on-disc tribometer (CSM THT) following ASTM G99. Pins (12 mm × 20 mm) machined from cured brake pad composites were slid against a 300 mm diameter hardened steel disk (R_a 0.2 µm) under normal loads of 30 N and 50 N at sliding speeds of 0.5 m/s and 1.0 m/s over a 1000 m distance. Mass loss before and after the tests determined the wear volume. At the same time, a piezoelectric sensor recorded the friction force to calculate the coefficient of friction in both dry and wet (5% solution of H_2O) conditions.

2.3.4 Morphological Studies

Morphological analysis of the fractured and worn surfaces was performed using SEM on a Zeiss Sigma 300 at 5 kV. The specimens were sputter-coated with a 5 nm gold layer. SEM images at 200x and 2000x magnifications elucidated the filler dispersion, matrix–filler interface quality, and wear mechanisms (e.g., abrasive grooves, delamination, and transfer films). Combined, these characterization techniques provide comprehensive insights into the mechanical, tribological, and microstructural behaviors of the eco-friendly brake pad composites.

3. RESULTS AND DISCUSSION

3.1 FTIR Analysis of CPH Nano-fillers

The FTIR spectrum of the nano-CPH fillers is presented in Fig. 2. Several distinct absorption bands corresponding to the characteristic functional groups of lignocellulosic biomasses are evident. The broad band observed around 3400 cm^{-1} corresponds to the O–H stretching vibration, which is attributed to the hydroxyl groups present in cellulose, hemicellulose, and lignin, as well as hydrogen-bonded water molecules. The intensity of this band reflects the hydrophilic nature of the CPH particles owing to their abundant hydroxyl moieties, which play a critical role in matrix–filler hydrogen bonding during composite formation.

The absorption peak near 2920 cm^{-1} is assigned to aliphatic C–H stretching vibrations, mainly from the methyl and methylene groups in the cellulose and lignin structures. These C–H vibrations are indicative of the hydrocarbon backbone of the polysaccharide chains and the aromatic network of lignin. A prominent peak at approximately 1740 cm^{-1} corresponds to C=O stretching vibrations, which are characteristic of unconjugated carbonyl groups present in hemicellulose acetyl esters or ester linkages in lignin. The presence of this carbonyl signal indicates that the nano-filler retains its native ester functionalities, which can enhance interfacial adhesion with polar resin systems via dipole–dipole interactions.

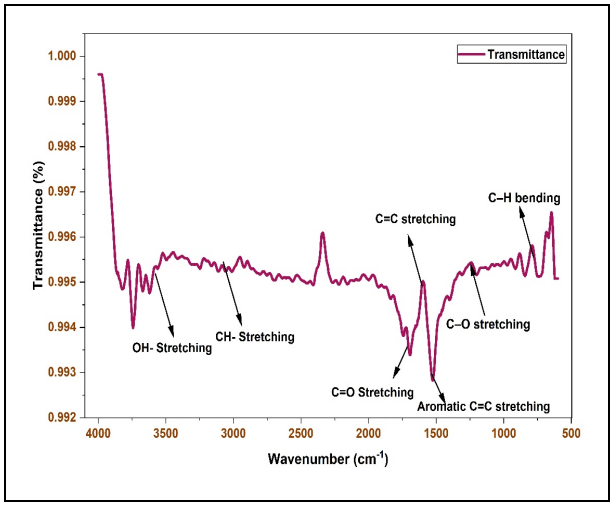


Fig. 2: FTIR analysis of CPH nanofillers

The absorption band around 1620–1640 cm^{-1} is assigned to C=C stretching in aromatic rings, arising from the lignin fraction, and may also overlap with the bending modes of adsorbed water. This aromatic signal confirms the structural integrity of lignin after mechanical size reduction. A peak in the region of 1240–1020 cm^{-1} is attributed to C–O stretching vibrations in cellulose and hemicellulose, representing ether linkages and C–O–C glycosidic bonds, respectively. These

polysaccharide-specific vibrations confirm the cellulose-rich composition of the CPH nanofillers. Finally, the band detected below 700 cm^{-1} is associated with C–H out-of-plane bending in aromatic structures, further confirming the contribution of lignin to the chemical profile of the fillers.

The preservation of these functional groups after high-energy ball milling suggests that the nanosizing process did not significantly degrade the chemical composition of CPH. The presence of abundant hydroxyl, carbonyl, and aromatic groups provides multiple active sites for interaction with epoxy matrices, potentially enhancing the filler–matrix adhesion through hydrogen bonding, van der Waals interactions, and covalent linkages during curing. Such chemical compatibility is expected to improve the stress transfer efficiency and mechanical reinforcement in brake pad composites.

3.2 XRD Analysis of CPH Nanofillers

The XRD pattern of the nano-CPH fillers is shown in Fig. 3. Two distinct diffraction peaks were observed at 2θ = 19.70° and 2θ = 39.16°, corresponding to the (110) and (220) planes, respectively. These peaks are characteristic of the semicrystalline cellulose I structure commonly found in lignocellulosic biomass. The prominent diffraction peak at 19.70° indicates the presence of ordered cellulose microfibrils within the CPH. In contrast, the smaller peak at 39.16° represents higher-order lattice reflections, confirming the preservation of crystalline domains after the high-energy ball milling process. The broad hump between these peaks represents the amorphous region, arising from the hemicellulose, lignin, and amorphous cellulose fractions.

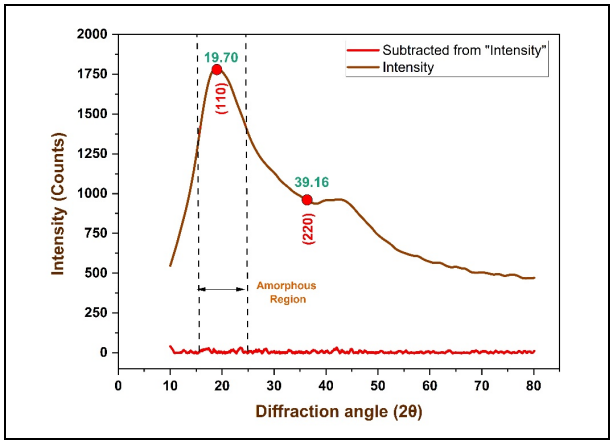


Fig. 3: XRD analysis of CPH nanofillers

The crystallinity index (CrI) was calculated using the peak deconvolution method, reflecting the relative proportion of crystalline cellulose in the material. The moderate crystallinity observed suggests that mechanical milling induced partial disruption of the ordered cellulose domains, thereby increasing the amorphous content. This increase in the number of amorphous regions can improve the filler–matrix compatibility by enhancing the surface reactivity and wettability during composite fabrication. Furthermore, the crystallite size, determined using the Scherrer equation, indicated nanoscale cellulose domains, which are consistent with the particle size reduction achieved through ball milling. The combination of crystalline cellulose (providing mechanical reinforcement) and amorphous regions (enhancing interfacial bonding) is advantageous for composite applications because it balances stiffness with improved adhesion to the polymer matrix. Overall, the XRD results confirmed that the CPH nanofillers retained essential crystalline cellulose structure while exhibiting an increased amorphous fraction, both contributing positively to their reinforcing potential in epoxy-based brake pad composites.

3.3 Particle Size Analysis of CPH Nanofillers

The particle size distribution of the CPH nanofillers was determined using ImageJ analysis of the SEM micrographs (Fig. 4a), which reveals irregularly shaped particles with a relatively wide size range, indicating heterogeneous fragmentation of the lignocellulosic structure during high-energy ball milling. The histogram in Fig. 4b shows that the particle sizes followed an approximately normal distribution, with the majority of particles falling between 2 and 6 µm in length. Statistical analysis (Fig. 4c) yielded an average particle length of 4.53 µm, with a standard deviation of 1.85 µm, a minimum size of 2.22 µm, and a maximum size of 9.88 µm. The observed particle size variation can be attributed to the differences in mechanical resistance between the cellulose-rich crystalline regions and amorphous lignin/hemicellulose domains, which fracture differently under milling forces.

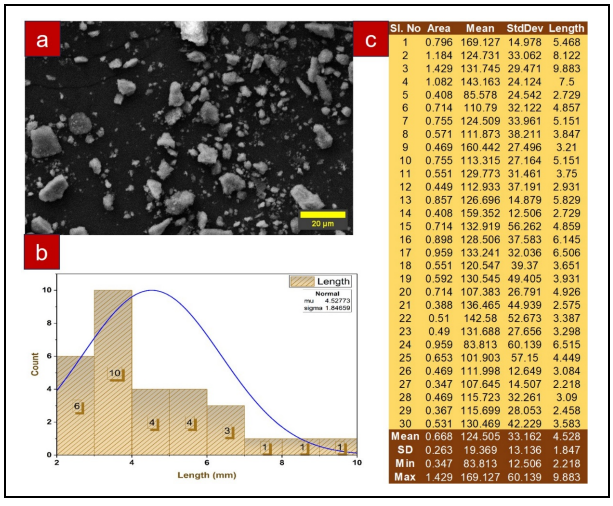


Fig. 4: Particle size analysis of CPH nanofillers: (a) SEM image, (b) Distribution plot, and (c) Particle size distribution chart

The nanoscale particle size, combined with a relatively narrow distribution, is advantageous for reinforcing composites. Smaller particles provide a higher surface area-to-volume ratio, enhancing interfacial bonding with the epoxy matrix and facilitating a uniform filler dispersion. This can reduce stress concentration zones, improve load transfer, and contribute to the enhanced mechanical properties of the brake pad composites. Furthermore, particles within the 2–6 µm range are small enough to effectively penetrate the polymer matrix network while avoiding excessive agglomeration, which can occur with ultrafine nanoparticles. Consequently, the particle size analysis verified that the high-energy milling process effectively reduced the CPH from micron-sized (more than 10 µm) to submicron dimensions (below 10 µm), resulting in a morphology conducive to mechanical reinforcement in high-performance, eco-friendly brake pad composites.

3.4 Effect of Nano-CPH on Mechanical Properties

3.4.1 Tensile Strength

Fig. 5 shows the tensile strengths of the brake pad composites with varying nano-CPH contents. The tensile strength increased significantly from 13.6 MPa for Composition 1 (31 wt. % CPH) to 31.2 MPa in Composition 3 (21 wt. % CPH), representing a 129.4% improvement. This trend can be attributed to the improved filler dispersion and stronger interfacial bonding achieved at moderate nano-CPH loadings. At higher concentrations (e.g., 31 wt. % in Composition 1), particle agglomeration likely occurred, creating microstructural defects that hindered stress transfer.

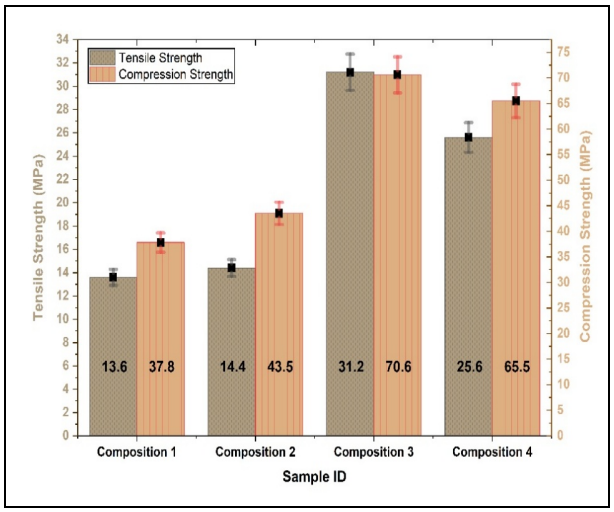


Fig. 5: Tensile and compressive strengths of the developed composites

The optimal performance was achieved at 21 wt. % (Comp. 3) suggests that this level of nano-CPH effectively reinforces the epoxy matrix without introducing defects, facilitating stress distribution through the cellulose domains and enhancing toughness via lignin content; a further decrease to 16 wt. % in Comp. 4 led to a slight reduction in tensile strength, indicating insufficient filler reinforcement despite better dispersion.

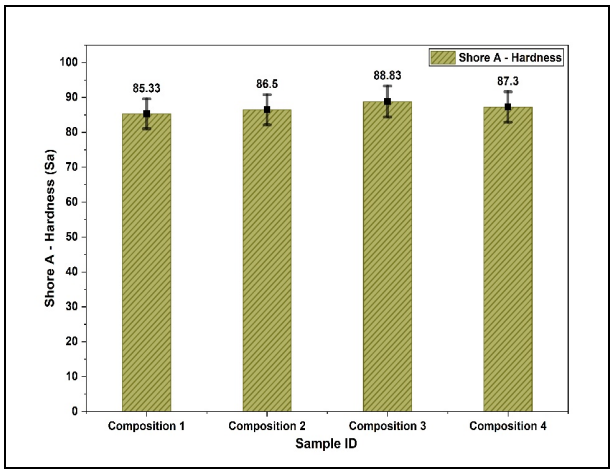


Fig. 6: Shore a hardness of the developed composites

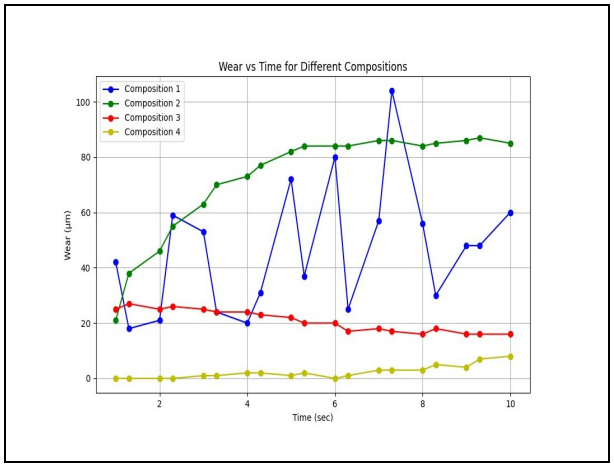


Fig. 7: Wear behavior of the nano-CPH-reinforced composites

3.4.2 Compressive Strength

The compressive strength followed a similar trend, as shown in Fig. 5, increasing from 37.8 MPa (Comp. 1, 31 wt. % CPH) to a peak of 70.6 MPa (Comp. 3, 21 wt. % CPH). This 86.8% increase highlights the reinforcing effect of well-dispersed nano-CPH, which acts as micro-pillars resisting deformation. Nanoscale particles improve dimensional stability and stiffness through enhanced matrix interactions. At the highest filler loading (Comp. 1), excessive particles formed clusters that disrupted the stress pathways. Conversely, at the lowest loading (Comp. 4, 16 wt. % CPH), the reduced filler content limited reinforcement potential, lowering compressive strength slightly to 65.5 MPa, though it remained substantially higher than the baseline.

3.4.3 Hardness

The Shore A hardness values, shown in Fig. 6, increased moderately from 85.33 (Comp. 1) to a maximum of 88.83 (Comp. 3), accounting for a 4.1% improvement. The hardness enhancement is due to the restriction of polymer chain mobility at the surface by the well-dispersed nano-CPH particles. However, because hardness testing only assesses near-surface behavior, the improvement is less pronounced than that in the tensile or compressive strength. Composition 4 (16 wt. % CPH) showed a slight reduction in hardness, correlating with the reduced nano-filler content. Overall, the data confirm that moderate nano-CPH loadings enhance both the surface and bulk mechanical performance.

3.5 Tribological Behavior

3.5.1 Wear Behavior

Fig. 7 illustrates the wear depth profiles under dry sliding conditions. Composition 1 (31 wt.% % CPH) exhibited the highest wear, with fluctuating values between 18 µm and 104 µm. This instability is linked to poor matrix–filler interactions and weak cohesion, resulting in rapid material loss and inconsistent friction film formation. Composition 2 (26 wt.% %) showed improved but still significant wear (~85 µm), suggesting partial reduction in agglomeration. The most favorable wear resistance was achieved with Composition 4 (16 wt% CPH), with a wear of as low as 8 µm, indicating that a lower filler content led to a more uniform dispersion and better transfer film stability.

Although Composition 3 (21 wt.% %) showed slightly higher wear (~15 µm), it maintained a stable and gradual wear trend, indicating effective formation of a lubricious transfer layer. The lignin-rich CPH particles contributed carbonaceous residues, enhancing self-lubrication and protecting the composite surface. Thus, while Composition 4 had the least wear, the combination of low wear and mechanical strength in Composition 3 made it the most balanced formulation.

3.5.2 Friction Force Behavior

The friction force behavior, as shown in Fig. 8, varies significantly across the formulations. Composition 1 (31 wt.% %) exhibited the lowest and most erratic friction forces (3.0–5.5 N), caused by poor filler dispersion and unstable contact at the sliding interface. Composition 2 (26 wt.% %) showed improved friction (starting at 7.4 N and rising to 9.8 N), with reduced oscillations, indicating better contact conditions due to more uniform filler distribution. Composition 3 (21 wt.% %) delivered the highest and most stable friction force, increasing from 10.2 N to 17.5 N, with a minor dip at 7 seconds due to transient film rearrangement. This superior performance is attributed to the formation of a stable carbon-rich transfer film derived from nano-CPH, which resists metal–polymer adhesion and maintains consistent friction. Composition 4 (16 wt.% %) maintained relatively high but slightly lower friction force levels (5.7–9.2 N) compared to Composition 3, likely due to reduced filler quantity limiting the buildup of a thick lubricating film. In summary, 21 wt. % nano-CPH (Composition 3) represents the optimum balance, offering high and consistent friction forces through effective tribolayer formation, while minimizing wear and maximizing mechanical performance.

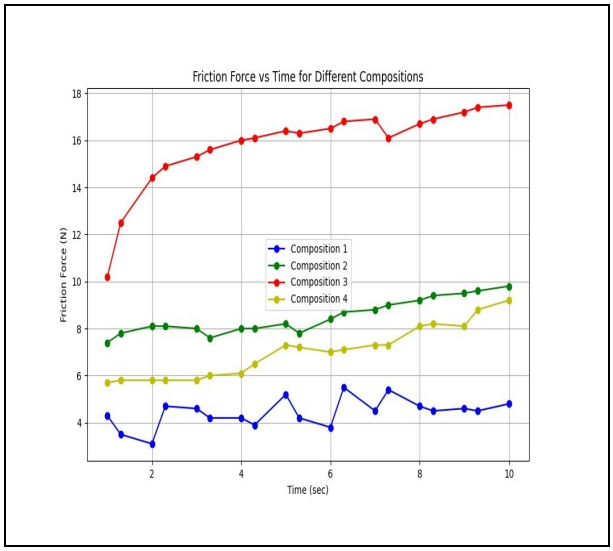


Fig. 8: Friction force behavior of the nano-CPH-reinforced composites

3.6 Scanning Electron Microscopy (SEM) Analysis

The surface morphologies of the fractured brake pad composites were examined using SEM to understand the dispersion behavior, filler-matrix interaction, and wear mechanisms of nano-CPH at different compositions. Fig. 9 (a–d) shows representative micrographs of Compositions 1–4.

The microstructure of Composition 1 revealed significant agglomeration of nano-CPH particles, which formed large clusters embedded within the epoxy matrix. These agglomerates disrupt the continuity of the polymer matrix, creating stress concentration sites and microvoids that serve as crack-initiation points under mechanical loading. This morphological feature corresponds to the low tensile strength and high wear rate observed for this composition, as discussed previously. The lack of uniform dispersion also suggests that the filler content exceeded the optimal loading capacity of the matrix, leading to inefficient stress transfer and a reduction in interfacial bonding. Consequently, the composite exhibited brittle failure patterns and poor tribological performance, confirming that excessive filler loading is detrimental to both structural integrity and friction stability.

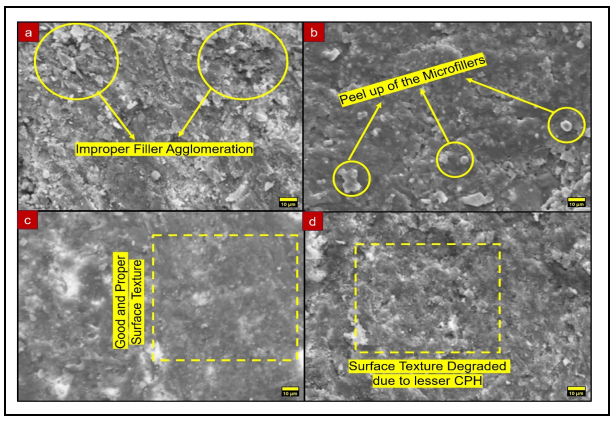


Fig. 9 (a-d): SEM images of compositions 1–4 of the developed nano-CPH-reinforced composites

Composition 2 exhibited a microstructure indicative of microfiller detachment and surface peeling, as evidenced by the presence of multiple voids and pits. These features are indicative of weak interfacial adhesion between the matrix and filler particles, causing the filler particles to be dislodged during mechanical or tribological loading. Although the agglomeration was less severe than that in Composition 1, the presence of detached fillers suggests that the nano-CPH content was still relatively high, compromising the matrix's ability to adequately wet and encapsulate all filler particles. This corresponds to the moderate mechanical performance and elevated wear rate, as the detachment of fillers can lead to third-body abrasion and instability in the friction layer during braking.

The SEM image of Composition 3 reveals a uniform and compact surface morphology with no visible agglomeration or peeling of the active material. This suggests a homogeneous dispersion of nano-CPH within the epoxy matrix and strong interfacial adhesion, allowing efficient stress transfer and energy dissipation during mechanical loading. The surface texture was smooth and continuous, which supports the formation of a stable transfer film during sliding, enhancing both wear resistance and friction stability. These features correlate with the highest tensile and compressive strengths, best wear performance, and most stable friction behavior observed experimentally. Composition 3 was identified as the optimum formulation, combining mechanical robustness with excellent tribological characteristics owing to its well-dispersed nano-CPH content.

For Composition 4, the SEM image shows a somewhat degraded surface texture, with regions of lower particle density and minor surface roughness irregularities. Although agglomeration is absent, the insufficient nano-CPH content leads to under-reinforcement of the matrix, resulting in less mechanical interlocking and a reduced load-bearing capacity. The decreased filler content limited the ability to form a continuous protective transfer layer during sliding, slightly affecting the tribological performance, as observed in the modest reduction in the friction force and hardness. Nonetheless, the wear resistance remained high owing to the lack of agglomerates, but the overall mechanical performance slightly decreased compared to that of Composition 3. Table 3 shows the SEM and its implications.

Table 3. SEM and its implications

Composition	CPH Content	SEM Observation	Implication
Composition 1	31 wt. %	Agglomeration of fillers	Poor dispersion, weak interface, high wear
Composition 2	26 wt. %	Microfiller peeling, voids	Weak adhesion, moderate wear, and friction
Composition 3	21 wt. %	Uniform dispersion, smooth texture	Optimal bonding, best mechanical/tribological
Composition 4	16 wt. %	Slightly degraded texture, less filler	Good wear, lower strength due to low CPH

The SEM study confirmed that filler dispersion and content are critical in determining the performance of nano-CPH-reinforced brake pad composites. Excessive filler leads to agglomeration and interfacial weakness, whereas insufficient filler fails to reinforce the matrix adequately. The optimal nano-CPH content was 21 wt. %, balancing particle dispersion and matrix interaction to achieve enhanced mechanical strength, wear resistance, and stable friction behavior.

3.7 Mechanical and Tribological Properties: Comparative Discussion

The mechanical performance of the nano-CPH-reinforced brake pad composites demonstrated significant improvement across all evaluated parameters, particularly at an optimal filler loading of 21 wt. % (Composition 3). The tensile strength showed a marked increase from 13.6 MPa for Composition 1 to a peak of 31.2 MPa in Composition 3. This enhancement is attributed to the homogeneous dispersion of the nano-CPH particles and strong interfacial bonding with the epoxy matrix, which enabled efficient stress transfer and reduced the occurrence of stress concentration zones. When compared with previous studies, this tensile strength surpasses that of brake pads reinforced with carbonized bamboo culms, which recorded only 10.3 MPa, as reported by Dagwa *et al.* (2025). Similarly, Olabisi (2016) achieved only 12.0–15.7 MPa with cocoa bean shell fillers, whereas the hybrid sisal-jute composites studied by Manjulaiah *et al.* (2024) did not exceed 25 MPa. This positions nano-CPH as a superior biofiller in terms of tensile performance.

The compressive strength followed a similar trend, reaching a maximum of 70.6 MPa for Composition 3. This value is significantly higher than those observed

in comparable green composites, such as the rice husk–epoxy composite system reinforced with Al_2O_3 and Fe_2O_3, which achieved a maximum of 58 MPa (Khafidh *et al.* 2023). Additionally, candlenut and coconut shell composites investigated by Juan *et al.* (2020) reached compressive strength levels of only ~45 MPa. In contrast, bush mango shell composites reported by Onyenanu *et al.* (2024) were limited to 51–55 MPa. The superior compressive behavior of the nano-CPH composites can be attributed to the nanoscale particle size, which promotes better particle packing and reduces porosity, thereby enhancing the load-bearing capacity. Moreover, the lignin content of CPH provides additional stiffness and dimensional stability.

Table 4. Comparison of mechanical and tribological properties of nano-CPH brake pad composite with previously reported bio-based brake pad materials

Property	Nano-CPH (Current study)	Bamboo (Dagwa *et al.* 2025)	Cocoa Shell (Olabisi, 2016)	Rice Husk (Khafidh *et al.* 2023)	Sisal-Jute (Manjulaiah *et al.* 2024)	Molluscan Shell (Jiyas *et al.* 2025)
Tensile Strength (MPa)	31.2	10.3	15.7	20–23	<25	22–26
Compressive Strength (MPa)	70.6	Not reported	50	58	65	60–68
Hardness (Shore A)	88.83	80–85	82	82–86	86	87–90
Wear Depth (µm)	8–15	0.15 mm³/Nm	Not reported	10–12	15	6–9
Friction Force (N)	17.5	12	10–13	11–14	14–16	16–18

In terms of surface hardness, Composition 3 exhibited the highest Shore A hardness of 88.83. This value is comparable to or slightly exceeds those reported in other studies, such as 80–85 for bamboo-based composites and 82–86 for rice husk-based composites. Cocoa shell-based composites, on the other hand, demonstrated lower hardness values, ranging from 78 to 82. The higher hardness of the nano-CPH composites reflects the reinforcement effect of the finely dispersed filler particles, which restrict the mobility of the polymer chains and increase the resistance to indentation. This is especially beneficial in applications where abrasive resistance is essential for maintaining the integrity of the brake pad during operation.

The tribological evaluation revealed that Composition 4 (16 wt. % CPH) exhibited the lowest wear depth of approximately 8 µm, likely due to improved filler dispersion and minimal agglomeration. However, Composition 3, with a wear depth of 15 µm, exhibited the best overall balance of mechanical strength and wear resistance. These results outperform those of several natural filler composites documented in the literature. For example, rice husk composites exhibited wear depths of approximately 10–12 µm, and carbonized bamboo culm-based composites demonstrated volumetric wear rates of roughly 0.15 mm³/Nm. Molluscan shell-based brake pads developed by Jiyas *et al.* (2025) exhibited wear rates in a similar range (6–9 µm), depending on the shell type. The enhanced wear resistance in the nano-CPH system was attributed to the formation of a stable carbonaceous transfer layer on the contact surface during sliding, derived from the lignin component of the rice husk. This transfer layer reduces the direct contact with the steel disc, thereby minimizing the material removal and surface degradation. Table 4 shows a comparison of the mechanical and tribological properties of the nano-CPH brake pad composite with previously reported bio-based brake pad materials.

Friction behavior analysis further confirmed the superior performance of the nano-CPH composite. Composition 3 exhibited the highest and most stable friction force, reaching 17.5 N. This level of stability surpasses that of many conventional bio-based composites, including cocoa shell pads (10–13 N), rice husk pads (11–14 N), and sisal-jute hybrids (14–16 N). Even molluscan shell-based pads, while achieving up to 18 N in some cases, lack the consistent friction force observed in nano-CPH pads. The excellent frictional behavior of the nano-CPH composites is linked to the synergistic effect of the nano-filler reinforcement and lignin-based surface films, which reduce the stick-slip behavior and enhance the friction stability under dynamic loading. These results are particularly significant for real-world brake applications, in which consistent friction is critical for vehicle safety and performance.

In summary, the nano-CPH brake pad composite developed in this study (particularly at 21 wt. % filler loading) exhibits superior mechanical and tribological properties when benchmarked against previously studied bio-based brake pads. The combination of high tensile and compressive strengths, excellent surface hardness, reduced wear, and stable friction force confirms the effectiveness of nano-CPH as a sustainable, high-performance filler for eco-friendly brake-pad applications. These findings not only highlight the technical advantages of nano-CPH over other natural fillers but also support its potential for industrial-scale adoption in green automotive-friction materials.

4. CONCLUSION

This study successfully developed and evaluated eco-friendly brake pad composites reinforced with nanosized cocoa pod husks, highlighting their potential as sustainable alternatives to conventional friction materials. The key findings demonstrate that the incorporation of nano-CPH significantly enhanced the

mechanical and tribological performance of the brake pads, with notable improvements in the tensile strength, compressive strength, surface hardness, and friction stability. Among the various formulations, the optimal composition was achieved at 79 wt. % epoxy and 21 wt. % nano-CPH, which delivered the best overall balance of strength, wear resistance, and consistent friction behavior. The improved performance was attributed to the uniform dispersion of nano-CPH, adequate interfacial bonding, and formation of a stable transfer film during braking. These results underscore the viability of using agricultural waste, such as cocoa pod husks, for green engineering applications, promoting both environmental sustainability and functional performance in automotive components. However, some commercial ceramic pads combine high friction with low wear, good hardness, and strong heat tolerance. In comparison, the nano-CPH composites can approach similar friction levels and offer biodegradability, but often exhibit lower mechanical strength. Thus, while nano-CPH brake pads are promising as eco-friendly alternatives, achieving the commercial benchmarks for friction stability and fade resistance will require further development (e.g., improved binders or hybrid fillers).

4.1 Recommendations

To further validate the practical application of nano-CPH brake pads, additional studies are recommended at elevated temperatures and varying humidity levels:

- Conducting long-term durability tests and investigations into noise and vibration behavior during braking cycles.
- Scaling up the formulation for commercial brake pad production and evaluating its performance under industry-standard tests.

FUNDING

This research received no specific grant from any funding agency in the public, commercial, or not-for-profit sectors.

COPYRIGHT

This article is an open-access article distributed under the terms and conditions of the Creative Commons Attribution (CC BY) license (http://creativecommons.org/licenses/by/4.0/)



CONFLICTS OF INTEREST

The authors declare that there is no conflict of interest.

REFERENCES

Adetunji, O. R., Adedayo, A. M., Ismailia, S. O., Dairo, O. U., Okediran, I. K., and Adesusi, O. M., Effect of silica on the mechanical properties of palm kernel shell-based automotive brake pad, *Mech. Eng, Soc, Ind.,* 2(1), 7–16(2022). https://doi.org/10.31603/mesi.6178

Ahmad, A., Moeed, A., Tariq, A., Nawab, Y., Farooq, M. U., and Umair, M., Effect of Hybridization Approach on Mechanical Performance of Jute-hemp/epoxy Hybrid Composite Laminates, *J. Nat. Fibers.,* 19(16), 14449-14460(2022). https://doi.org/10.1080/15440478.2022.2064398

Ali, S., Kumar, N., Grewal, J. S. G., Thakur, V., Chau, K. W., and Kumar, M., Coconut waste fiber used as brake pad reinforcement polymer composite and compared to standard Kevlar-based brake pads to produce an asbestos-free brake friction material, *Polym. Compos.,* 43(3), 1518–1525(2022). https://doi.org/10.1002/pc.26472

Bhakuni, H., Muley, A. V.,, and Ruchika Fabrication, testing & analysis of particulate ceramic matrix composite for automotive brake pad application. *Mater. Today. Proc.,* S2214785323005084(2023). https://doi.org/10.1016/J.MATPR.2023.01.413

Chandradass, J., Surabhi, M. A., Sethupathi, P. B., and Jawahar, P., Development of low-cost brake pad material using asbestos-free sugarcane bagasse ash hybrid composites, *Mater. Today. Proc.,* 45, 7050–7057(2021). https://doi.org/10.1016/J.MATPR.2021.01.877

Chaturvedi, S., Kataria, A., Chaudhary, V., Verma, A., Jain, N., Sanjay, M.R., and Siengchin, S., Bionanocomposites reinforced with cellulose fibers and agro-industrial wastes, *Cellul. Fibre Reinf. Compos. Interface Eng.,* 317–342(2023). https://doi.org/10.1016/B978-0-323-90125-3.00017-3

Dagwa, I. M., Okeke, O. E., Zarmai, M. T., Omiogbemi, I. M. B., Adeleke, A. A., Ikubanni, P. P., and Omotosho, E., Carbonized Bamboo Culm-Based Composite Materials: Mechanical and Frictional Performance for Brake Pad Applications, *Int. J. Des. Nat. Ecodyn.,* 20(3), 501–514(2025). https://doi.org/10.18280/ijdne.200305

Dirisu, J. O., Okokpujie, I. P., Apiafi, P. B., Oyedepo, S. O., Tartibu, L. K., Omotosho, O. A., Ogunkolati, E. O., Oyeyemi, E. O. and Uwaishe, J. O., Development of eco-friendly brake pads using industrial and agro-waste materials, *J. Eng. Appl. Sci.,* 71(1), 55(2024). https://doi.org/10.1186/s44147-023-00345-y

Divakaran, D., Sriariyanun, M., Jagadeesan, R., Suyambulingam, I., Sanjay, M. R. and Siengchin, S., Isolation and characterization of an agro-industrial waste-based novel cellulosic micro fillers from mustard (Brassica juncea) seed oil cake: A waste to wealth approach, *Biomass. Convers. Biorefin.,* 14(18), 22921-22937(2023). https://doi.org/10.1007/S13399-023-04346-Y

Imran, A. I., Siregar, J. P., Rejab, M. R. M., Cionita, T., Hadi, A. E., Jaafar, J., Fitriyana, D. F. and Dewi, R., Opportunities and challenges in the sustainable integration of natural fibers and particles in friction materials for eco-friendly brake pads, *Mech. Eng. Soc. Ind.,* 4(3), 337–367(2024). https://doi.org/10.31603/mesi.12271

Jiyas, N., Akshay, S. D., Ardra, S. J., Sekhar, A. M. R., Jayakrishnan, M., Sasidharan, I. and Kumar, K. B., Harnessing molluscan shell waste for sustainable tribology by integrating biogenic fillers in eco-friendly brake pad development, *Sci. Rep.,* 15(1), 21804(2025). https://doi.org/10.1038/s41598-025-06775-3

Juan, R. S., Kurniawan, C., Marbun, J. and Simamora, P., Mechanical properties of brake pad composite made from candlenut shell and coconut shell, *J. Phys. Conf. Ser.,* 1428(1), 012018(2020). https://doi.org/10.1088/1742-6596/1428/1/012018

Kannan, G., Thangaraju, R., Suttiruengwong, S., Shanmugam, V., Rangappa, S. M., Sumesh, K. R., Kurien, R. A. and Siengchin, S., Effect of drilling process parameters on agro-waste-based polymer composites reinforced with banana fiber and coconut shell filler, *Biomass. Convers. Biorefin.,* https://doi.org/10.1007/s13399-024-06140-w

Khafidh, M., Putera, F. P., Yotenka, R., Fitriyana, D. F., Widodo, R. D., Ismail, R., Irawan, A. P., Cionita, T., Siregar, J. P. and Ismail, N. H., A Study on Characteristics of Brake Pad Composite Materials by Varying the Composition of Epoxy, Rice Husk, Al2O3 and Fe2O3, *Automot. Exper.,* 6(2), 303–319(2023). https://doi.org/10.31603/ae.9121

Kumar, A. A. J., Ramaseshan, N. P. A. and Lakshmanan, T., Tribological analysis on basalt/aramid hybrid fiber reinforced polyimide composites: An alternate brake pad material, *Tribol. Ind.,* 43(2), 334–347(2021). https://doi.org/10.24874/ti.912.06.20.12

Kumar, K. P., Lokeshwar, G., Reddy, C. U. K., Arunjyotis., Shetty, N., Shahabaz, S. M. and Nargis, T., Experimental investigation of mechanical properties and morphology of ramie, bamboo, and ramie-bamboo hybrid composites with silicon carbide and alumina nanofillers, *Mater. Res. Express.,* 12(2), 025306(2025). https://doi.org/10.1088/2053-1591/adb2e3

Lokeshwari, M., Sagar, P. V., Kumar, K. D., Thirupathy, D., Subbiah, R., Ganeshan, P., Seikh, A. H., Mohammed, S. M. A. K. and Christopher, D., Optimization and Tribological Properties of Hybridized Palm Kernel Shell Ash and Nano Boron Nitride Reinforced Aluminium Matrix Composites, *J. Nanomater.,* 2022(1), 8479012(2022). https://doi.org/10.1155/2022/8479012

Mahecha, M. G., Valdez, H. S., Peralta, E., Millan, E. C., Santana, T. J. M., Ramírez, M. G. L. and Chávez, C. C., Production and Characterization of Cellulosic Pulp from Mango Agro-Industrial Waste and Potential Applications, *Polym.,* 15(15), 3163(2023). https://doi.org/10.3390/POLYM15153163

Manjulaiah, H., Dhanraj, S., Basavegowda, Y., Lamani, L. N., Puttegowda, M., Rangappa, S. M. and Siengchin, S., A novel study on the development of sisal-jute fiber epoxy filler–based composites for brake pad application, *Biomass. Convers. Biorefin.,* 14(19), 23411–23423(2024). https://doi.org/10.1007/s13399-023-04219-4

Manoj, E., Selvakumar, G., Prakash, S. R. and Jacob, A., Characterization study on eco-friendly break pad material using sorghum husk-derived Si3N4 and biochar friction modifier, *Biomass. Convers. Biorefin.,* 14(4), 5735–5744(2024). https://doi.org/10.1007/s13399-023-04917-z

Nandiyanto, A. B. D., Hofifah, S. N., Girsang, G. C. S., Putri, S. R., Budiman, B. A., Triawan, F., and Al-Obaidi, A. S. M., The effects of rice husk particles size as a reinforcement component on resin-based brake pad performance: from literature review on the use of agricultural waste as a reinforcement material, chemical polymerization reaction of epoxy resin, to experiments, *Automot. Exper.,* 4(2), 68–82(2021). https://doi.org/10.31603/ae.4815

Nandiyanto, A. B. D., Husaeni, D. N. A., Ragadhita, R., Fiandini, M., Husaeni, D. F. A., and Aziz, M., Resin Matrix Composition on the Performance of Brake Pads Made from Durian Seeds: From Computational Bibliometric Literature Analysis to Experiment, *Automot. Exper.,* 5(3), 328–342(2022a). https://doi.org/10.31603/ae.6852

Nandiyanto, A. B. D., Ragadhita, R., Girsang, G. C. S., Anggraeni, S., Putri, S. R., Sadiyyah, F. H., Hibatulloh, M. R., Valensia. and Setiadi, D. P., Effect of palm fronds and rice husk composition ratio on the mechanical properties of composite-based brake pad, *Moroccan J. Chem.,* 10(4), 663–677(2022b). https://doi.org/10.48317/IMIST.PRSM/morjchem-v10i4.34291

Navaneethakrishnan, S., Sivabharathi, V. and Ashokraj, S., Weibull distribution analysis of roselle and coconut-shell reinforced vinylester composites, *Aust. J. Mech. Eng.,* 19(4), 457–466(2021). https://doi.org/10.1080/14484846.2019.1637089

Olabisi., A. I., Development and Assessment of Composite Brake Pad Using Pulverized Cocoa Beans Shells Filler, *Int. J. Mater. Sci. Appl.,* 5(2), 66(2016). https://doi.org/10.11648/j.ijmsa.20160502.16

Onyenanu, I. U., Ofili, I. and Owuama, K. C., Eco-Friendly Brake Pad Formulation Using Agro-Waste Derived Fillers: Bush Mango Nutshell and Palm Fruit Fiber Reinforced Composites, *Int. J. Appl. Nat. Sci.,* 2(2), 27–39(2024). https://doi.org/10.61424/ijans.v2i2.152

Pelissari, F. M., Mahecha, M. M. A., Sobral, P. J. D. A. and Menegalli, F. C., Nanocomposites based on banana starch reinforced with cellulose nanofibers isolated from banana peels, *J. Colloid. Interface. Sci.,* 505, 154–167(2017). https://doi.org/10.1016/J.JCIS.2017.05.106

Pradhan, P., Purohit, A., Singh, J., Subudhi, C., Mohapatra, S. S., Rout, D. and Sahoo, B. B., Tribo-performance Analysis of an Agro-Waste-Filled Epoxy Composites Using Finite Element Method, *J. Inst. Eng. (India) Ser. E.,* 103(2), 339–345(2022). https://doi.org/10.1007/S40034-022-00243-7

Prado, K. D. S. D. and Spinacé, M. A. D. S., Characterization of Fibers from Pineapple's Crown, Rice Husks and Cotton Textile Residues, *Mater. Res.,* 18(3), 530–537(2015). https://doi.org/10.1590/1516-1439.311514

Sivakumar, E. and Saju, K. K., Optimizing Brake Pad Performance of a Composite Materials Prepared with Smilax Zelanica/Glass Fiber and Nano Silica Across Diverse Sieve Variations, *Mater. Circ. Econ.,* 6(1), 28(2024). https://doi.org/10.1007/s42824-024-00122-z

Yashwanth, S., Mohan, M. M., Anandhan, R., and Selvaraj, S. K. Present knowledge and perspective on the role of natural fibers in the brake pad material, *Mater. Today. Proc.,* 46, 7329–7337(2021). https://doi.org/10.1016/J.MATPR.2020.12.995

Yigrem, M., Fatoba, O., and Tensay, S., "Tensile strength, wear characteristics, and numerical simulation of automotive brake pad from waste-based hybrid composite," *Mater. Today. Proc.,* 62(6), 2954–2964(2022b). https://doi.org/10.1016/j.matpr.2022.02.557

Yigrem, M., Fatoba, O. and Tensay, S., Tribological and mechanical properties of banana peel hybrid composite for brake-pad application, *Mater. Today. Proc.,* 62(6), 2829–2838 (2022a). https://doi.org/10.1016/j.matpr.2022.02.381

Yilma, W. M., Singh, B., Asrat, G., and Hossain, N., "Taguchi Method Optimization of Water Absorption Behavior by Wheat Straw-Basalt Hybrid Brake Pad Composite,″ *J. Compos. Sci.,* 7(2), 62(2023). https://doi.org/10.3390/jcs7020062